LA-UR- 12-01409

Approved for public release;
distribution is unlimited.

Title:	Full-scale fatigue tests of CX-100 wind turbine blades. Part II - analysis
Author(s):	Stuart G. Taylor *,** Hyomi Jeong***, Jae Kyeong Jang*** Kevin M. Farinholt*, Michael D. Todd**, Curtt Ammerman* * Los Alamos National Laboratory, Los Alamos, NM ** University of California, San Diego, La Jolla, CA *** Chonbuk National University, Korea
Intended for:	Proceedings of the SPIE Smart Structures/NDE Conference San Diego, CA, USA March 11-15, 2012

Los Alamos
NATIONAL LABORATORY
EST. 1943

Form 836 (7/06)

Full-scale fatigue tests of CX-100 wind turbine blades. Part II – analysis

Stuart G. Taylor*[a,b], Hyomi Jeong[c], Jae Kyeong Jang[c], Gyuhae Park[a], Kevin M. Farinholt[a], Michael D. Todd[b],Curtt M. Ammerman[a]

[a] Los Alamos National Laboratory, Los Alamos, NM;
[b] University of California, San Diego, La Jolla, CA
[c] Chonbuk National University, Korea

ABSTRACT

This paper presents the initial analysis results of several structural health monitoring (SHM) methods applied to two 9-meter CX-100 wind turbine blades subjected to fatigue loading at the National Renewable Energy Laboratory's (NREL) National Wind Technology Center (NWTC). The first blade was a pristine blade, manufactured to standard CX-100 design specifications. The second blade was manufactured for the University of Massachusetts, Lowell (UMass), with intentional simulated defects within the fabric layup. Each blade was instrumented with a variety of sensors on its surface. The blades were subject to harmonic excitation at their first natural frequency with steadily increasing loading until ultimately reaching failure. Data from the sensors were collected between and during fatigue loading sessions. The data were measured at multi-scale frequency ranges using a variety of data acquisition equipment, including off-the-shelf systems and prototype data acquisition hardware. The data were analyzed to identify fatigue damage initiation and to assess damage progression. Modal response, diffuse wave-field transfer functions in time and frequency domains, and wave propagation methods were applied to assess the condition of the turbine blade. The analysis methods implemented were evaluated in conjunction with hardware-specific performance for their efficacy in enabling the assessment of damage progression in the blade. The results of this assessment will inform the selection of specific data to be collected and analysis methods to be implemented for a CX-100 flight test to be conducted in collaboration with Sandia National Laboratory at the U.S. Department of Agriculture's (USDA) Conservation and Production Research Laboratory (CPRL) in Bushland, Texas.

Keywords: wind turbine, structural health monitoring, fatigue test, CX-100

1. INTRODUCTION

1.1 Overview

The authors have been investigating several design parameters of SHM techniques and the performance of high-frequency active-sensing SHM techniques, including wave propagation and diffuse wave-field transfer functions as methods to monitor the health of a wind turbine blade using piezoelectric sensors. In addition, a multi-scale sensing is proposed in order to assess the influence of structural damage on the low-frequency dynamic response of a blade. In order to implement these systems in the field, compact sensor nodes, which the authors have been developing [1-3], are necessary. To that end, prototype embedded sensing hardware is tested alongside commercial-off-the-shelf (COTS) data acquisition systems. With the proposed sensing strategy, a series of full scale fatigue tests were performed in collaboration with Sandia National laboratory and the National Renewable Energy Laboratory (NREL). These tests are a precursor for a planned full-scale deployment of an SHM system on CX-100 rotor blades to be flown in the field in collaboration with Sandia National Laboratory (SNL) at the U.S. Department of Agriculture's (USDA) Conservation and Production Research Laboratory (CPRL) in Bushland, Texas.

*sgtaylor@lanl.gov

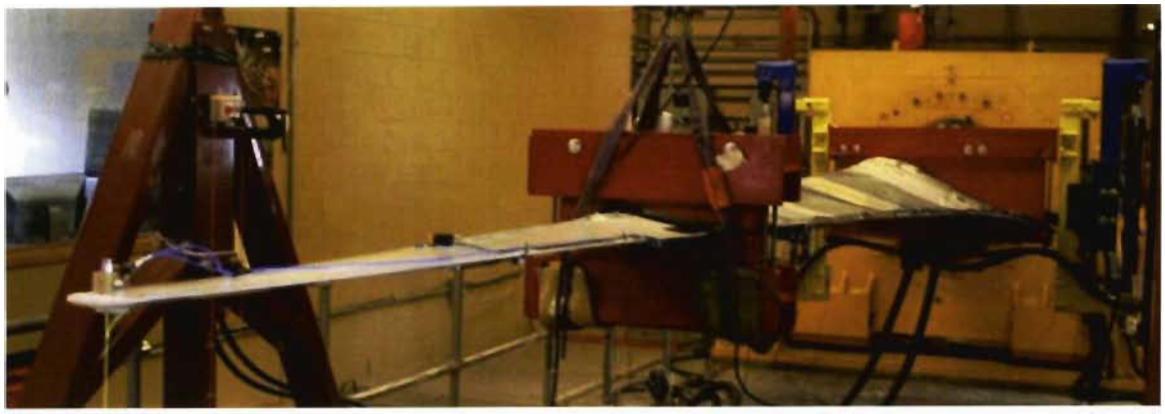

Figure 1. Test setup: a 9m CX-100 blade under a fixed-free condition

1.2 Test Structures

Two test structures were employed for fatigue testing. Each was a 9-m CX-100 blade [4], originally designed at Sandia National Laboratory. The first blade, dubbed the LANL blade, was manufactured according to standard specifications for the CX-100 blade. The LANL blade is shown mounted to the test fixture in Figure 1. The second blade, dubbed the University of Massachusetts, Lowell (UMass) blade, was manufactured with intentional defects. Each blade was mounted to a steel frame designed to approximate a fixed-free condition, and loads were introduced to the blade using a Universal Resonant EXcitation (UREX) system oscillating at the first resonant frequency of the blade.

1.3 Analysis Methods

Various methods were implemented using several data acquisition hardware systems; these systems are described in detail in our concurrent work [5]. The analysis methods considered were applied to wave propagation data using both diffuse waves and pulsed waves, which are characterized by propagating wave packets. Methods include principle component analysis of raw received signal, which was utilized for traveling wave analysis, prediction error using auto-regressive (AR) models, or ARX models (which include exogenous inputs) in the case of non-white noise excitation, correlation coefficients among frequency response functions (FRFs) in the diffuse wave field, and received power estimates. This paper presents a preliminary analysis of data collected in the course of the fatigue test. The techniques considered are not necessarily optimal detectors, but are a sampling of techniques commonly used in the literature for similar applications.

1.4 Blade Failure

The fatigue test began on 8/11/12, and it ran intermittently for approximately 8.5 million cycles until a fatigue crack became visible 11/8/12. The crack was a through-thickness crack that appeared on the surface of the blade in the root area on the leading edge. The area including the crack is shown in a photograph in Figure 2. The surfacing of this crack dramatically altered the dynamic characteristics of the blade, causing the blade's first resonance to vary as a function of loading. However, the authors believe that the damage that ultimately manifested itself as this externally visible crack was detectable using some of the methods applied in this paper as early as 10/20/12, approximately three weeks prior to the catastrophic failure. In the discussions to follow, the blade will be referred to as 'healthy' for the period prior to 10/20/12, 'transitionally damaged' for the period between 10/20/12 and 11/8/12, and 'catastrophically damaged' for the period after 11/8/12.

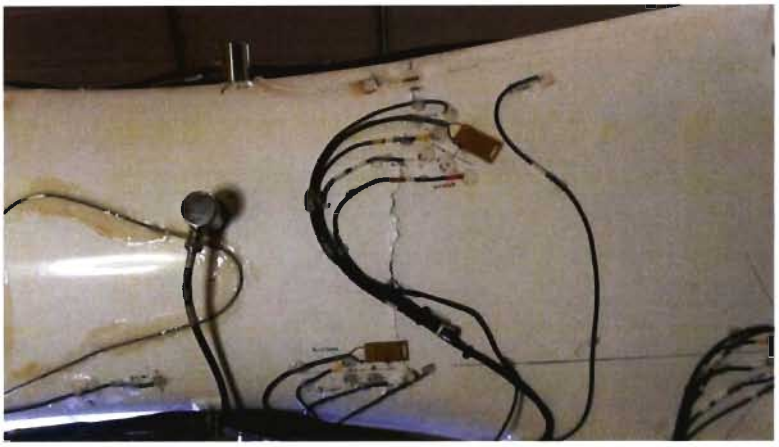

Figure 2. Photograph of fatigue crack in root area of blade.

2. SENSOR DIAGNOSTICS

2.1 Method Overview

The condition of a piezoelectric sensor mounted directly to a structure can be assessed by measuring the sensor's impedance over a relatively low frequency range, say from 5 kHz to 30 kHz, and computing the slope of the imaginary part of the admittance [6]. In this way, the health of the sensor can be assessed largely independently of the health of the underlying structure. Most active sensing methods focus on higher frequency ranges, say in the 50 kHz to 100 kHz range, because changes in structural behavior tend to be more pronounced at higher frequencies. Once a baseline has been established, or if there are enough sensors installed in the same configuration to act as an instantaneous baseline, this method permits a simple threshold algorithm to inform whether the sensor has broken, is becoming de-bonded from the structure, or its condition remains unchanged. An example measurement identifying the effect of each type of sensor failure is shown in Figure 3. Throughout the course of this fatigue test, the condition of the sensors was monitored using an HP 4291 impedance analyzer. However, more compact hardware can be utilized in order to perform this assessment, including low-power wireless devices [7].

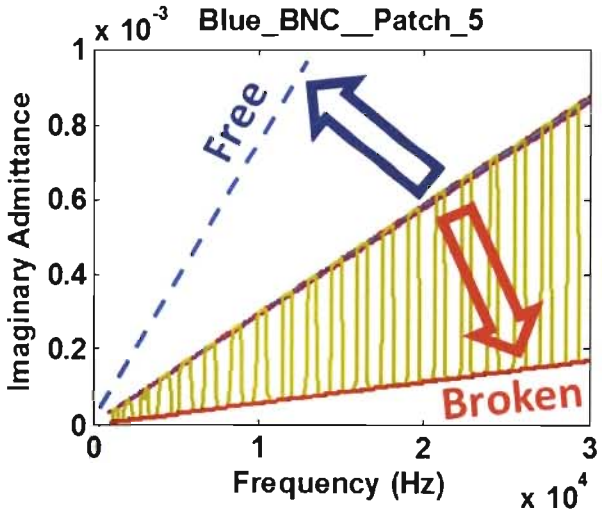

Figure 3. Depiction of sensor diagnostic measurement conclusions

2.2 Sensor Reliability and Longevity

The duration of this fatigue test was just over 12 weeks, exceeding by a factor of 3 the expected fatigue life of the blade. To the authors' knowledge, PZT sensors have not been subjected to extensive, real-world conditions for such a length of time. Throughout the course of the test, sensors failed and required replacement for a variety of reasons, including mundane cable breaks, but also de-bonding and ceramic cracking. For a long-term SHM system deployment, it is absolutely imperative that a sensor diagnostic capability be built in to the system. Sensor longevity should also be a consideration in the design of an SHM system, in terms of sensor construction and installation techniques.

2.3 Specific Diagnostic Examples

This section details some of the circumstances during the fatigue test in which sensors failed and required either repair or replacement. Figure 4 (left) shows the diagnostic data for a sensor that was replaced once near the end of the test. The replacement for this sensor survived through the end of the test. Figure 4 (right) shows a sensor that broke twice near the end of the test, possibly because of its close proximity to the site of the eventual catastrophic fatigue crack. This sensor was replaced once, but it was not replaced following its breaking at the end of the test.

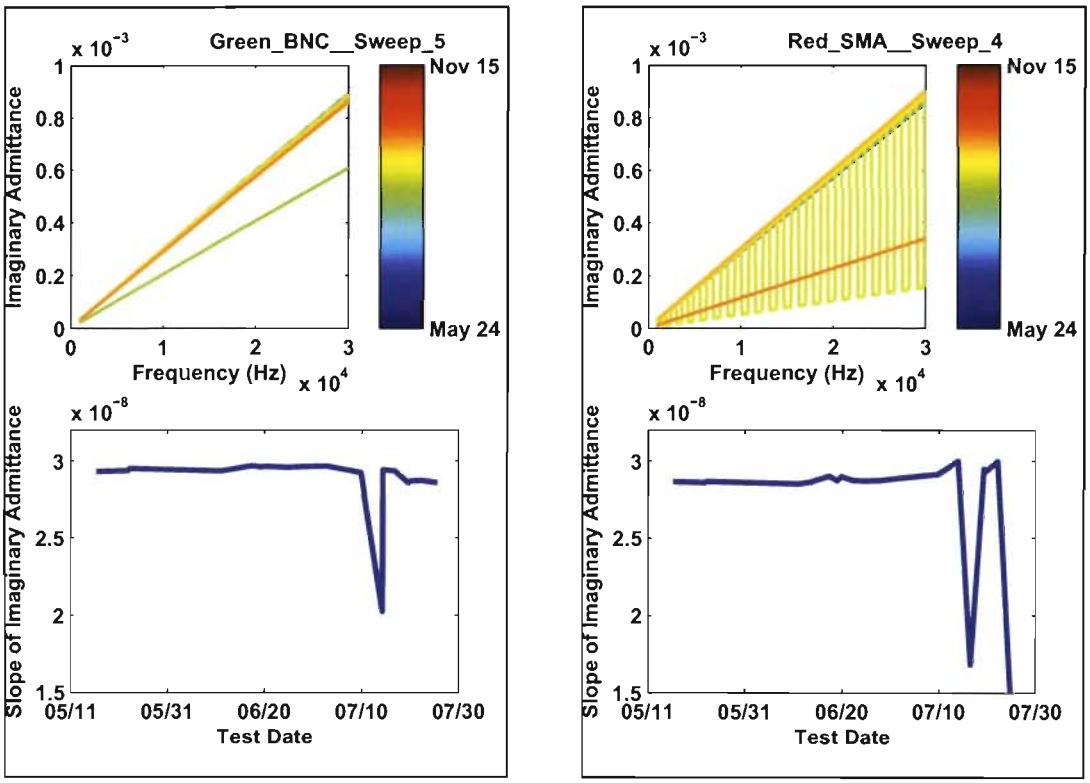

Figure 4. Sensor diagnostic measurement histories for sensors requiring either repair or replacement.

3. WAVE PROPAGATION METHODS

3.1 Principal Component Analysis

The method of applying principal component analysis (PCA) to the wave propagation data was first to isolate the received wave from the measured signal, and then transform that wave to the frequency domain by computing fast Fourier transform (FFT), so that the result is some function ϕ of power density. Sample figures for one sensor path depicting this process are shown in Figure 5.

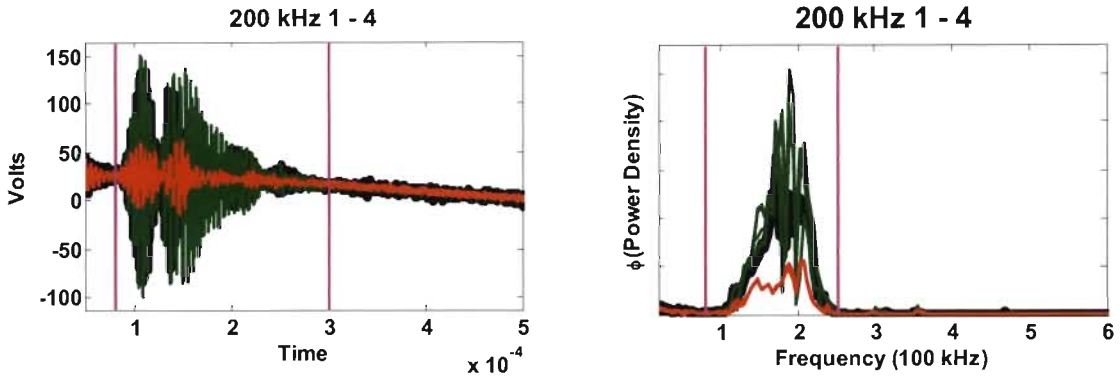

Figure 5. Raw and processed wave propagation data.

Treating the values of the FFT at each frequency line as a sample from a multivariate random distribution, the sample covariance matrix was calculated, and principle component loads were computed as the dot products of each FFT vector with the eigenvectors of the sample covariance matrix. The first and second principal component loads were plotted versus each other. Data drawn from two different high-dimensional multivariate distributions can often be separated by projecting them onto a lower-dimensional subspace in this way. Plots showing the PCA results for the low-pressure and high-pressure side arrays are shown in Figure 6 and Figure 7, respectively. Each plot includes an inset identifying the sensor paths, as well as the location of the damage on the low-pressure side, shown with a red line between sensors 4 and 5. In each PCA plot, the second principal component load is plotted versus the first. The loads computed using data taken from the blade in a healthy state are plotted in black, loads computed using data taken from the blade in the transition state are shown in green, and loads computed using data collected from the damaged blade are shown in red.

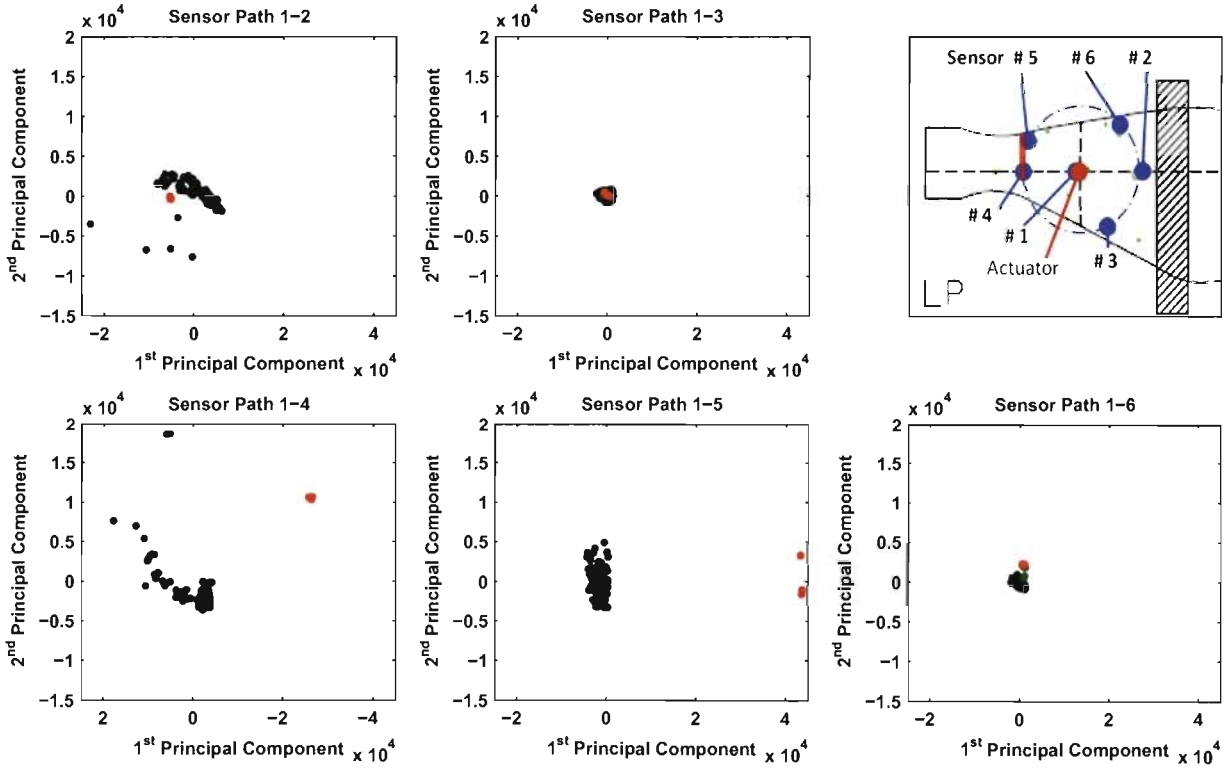

Figure 6. Wave propagation PCA results for the low-pressure side array.

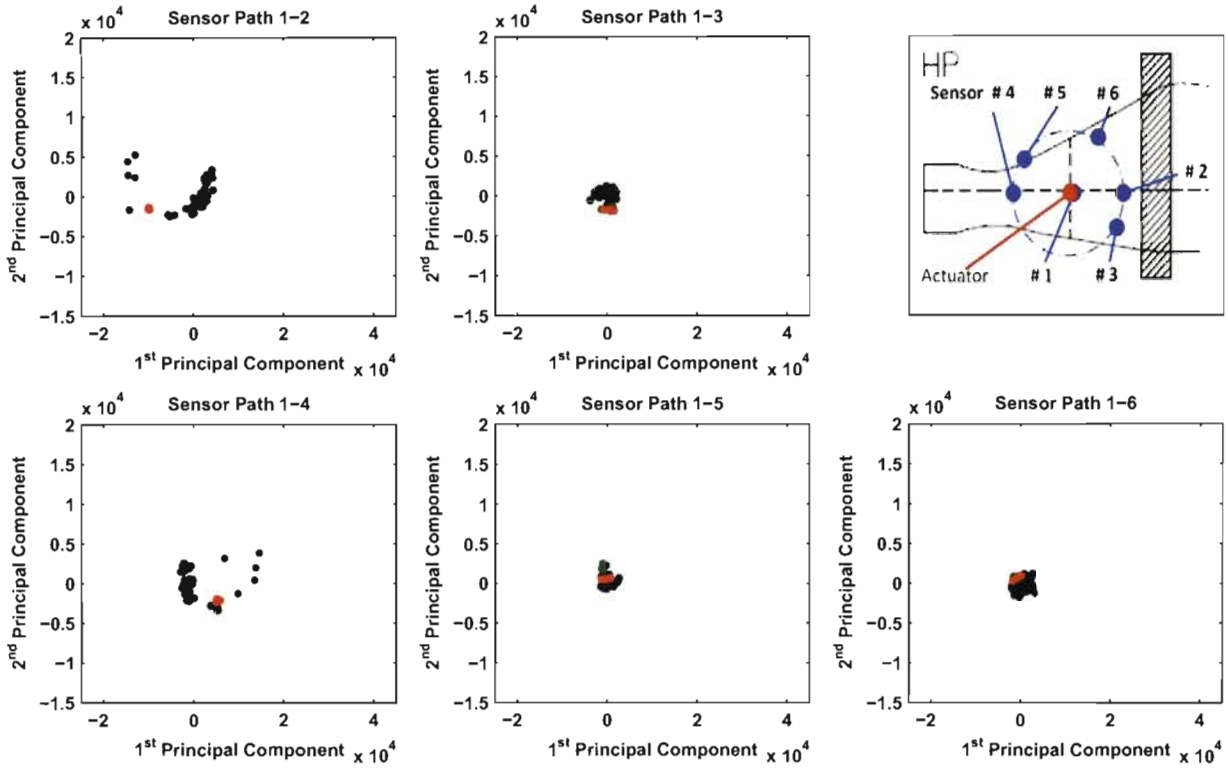

Figure 7. Wave propagation PCA results for the high-pressure side array.

On the low-pressure side, there is strong separation between the loads extracted from healthy blade data and those extracted from damaged blade data in sensor paths 1-4 and 1-5, correlating well with the actual location of the crack. The loads extracted from transitional blade data show moderate deviation from those for the healthy blade data, but not in a way that corresponds to the location of the developing damage. This method can successfully identify and locate the catastrophic damage, but does not seem effective in locating the transitional damage.

3.2 Received Wave Power

In the second method applied to the wave propagation data, a monotonic function of the received wave power in the frequency range of excitation was estimated by calculating the area under the FFT curve between 100 kHz and 250 kHz. Although data was collected over multiple frequency ranges, only the data with 200 kHz excitation are considered here. The results from this computation are shown for the low-pressure side and the high-pressure side arrays in Figure 8 and Figure 9, respectively. In each figure, there is an inset diagram indicating the sensor locations by number, as well as an indication of the damage location on the low-pressure side, given by a red line between sensors 4 and 5 on the low-pressure side. Furthermore, the received power feature values are plotted in black for healthy blade data, green for transitionally damaged blade data, and red for data from the failed bade. In Figure 8, there is a noticeable drop change in the received wave power for sensors 4 and 5 beginning with tests corresponding to Nov 8, following the catastrophic failure. However, the baseline measurements exhibit some non-stationary behavior prior to that point, making this feature somewhat difficult to use in detecting the transitionally damaged state.

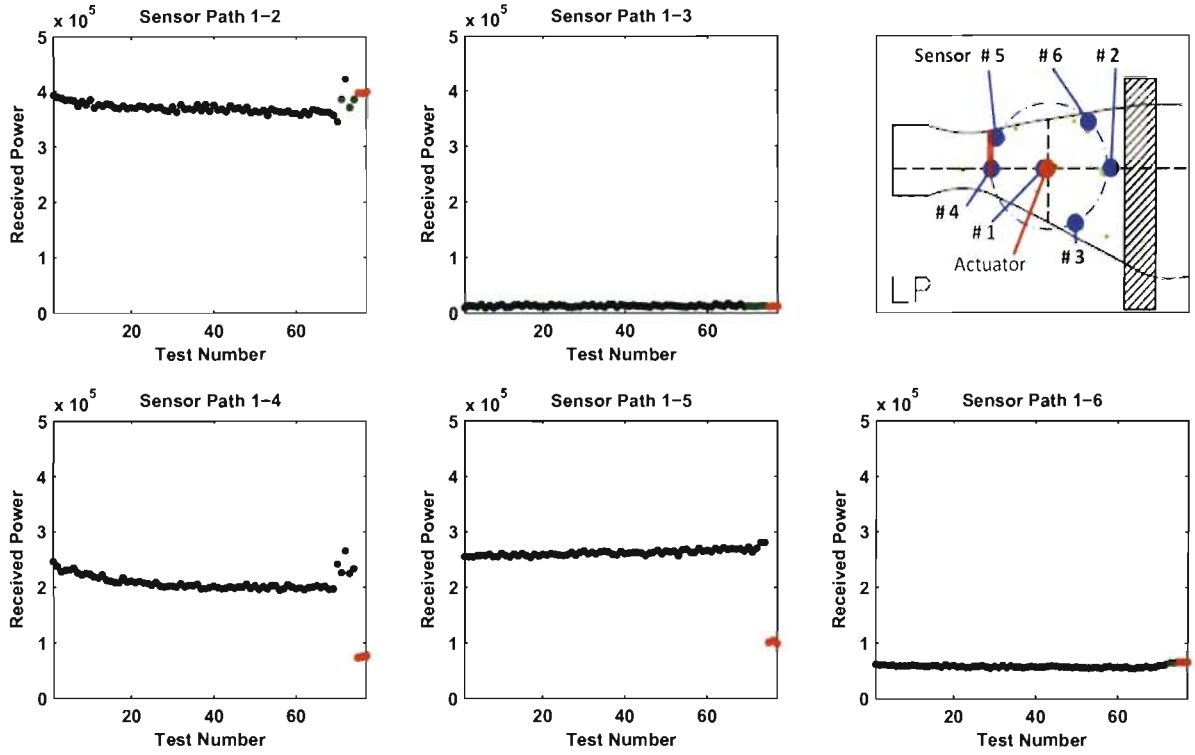

Figure 8. Received wave power results for the low-pressure side array.

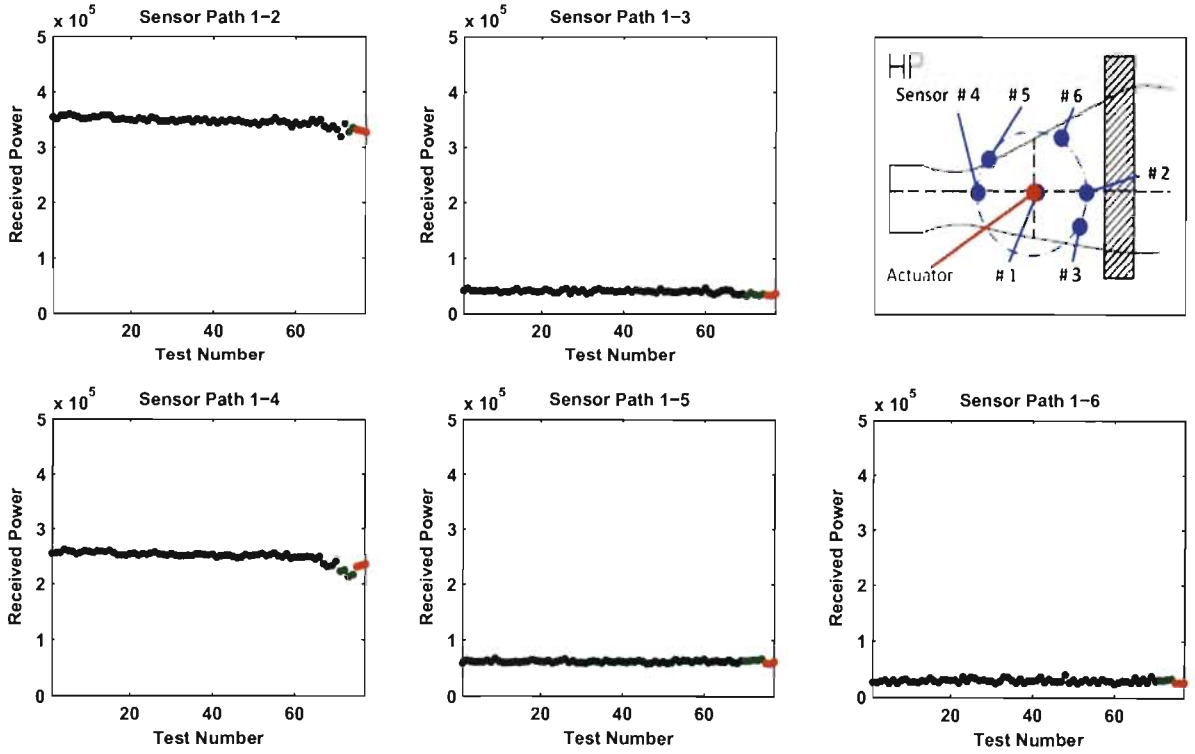

Figure 9. Received wave power results for the high-pressure side array.

4. DIFFUSE WAVE METHODS

4.1 ARX Model-based Principal Component Analysis

For the analysis of the WASP data, which were obtained using a chirp excitation, an ARX model of order (12,3) was fit to the data. The ARX model (with exogenous inputs) was required because the excitation was not white noise, so the process could not be modeled simply as autoregressive. Treating the model parameters as samples of a multivariate distribution, the covariance matrix was computed, and its eigenvectors were used to compute the principal component loadings for each set of model parameters. In this case, the covariance matrix was computed using only the baseline data, and the principle loads for all data were computed with respect to the baseline.

Plots showing the PCA results for the WASP data on the low-pressure side are shown in Figure 10, along with an inset identifying the sensor paths and the location of the fatigue crack, which was between sensors 4 and 5. In each plot, the blue dots were computed from data taken prior to Oct. 20, and the red dots were computed from data taken after Oct. 20. There is very little separation in the data for paths 1-2, 1-3, and 1-6, but there is near complete separation in the data for paths 1-4 and 1-5, which were physically nearest the crack. This method appears as though it is sensitive to local structural changes while still permitting localization.

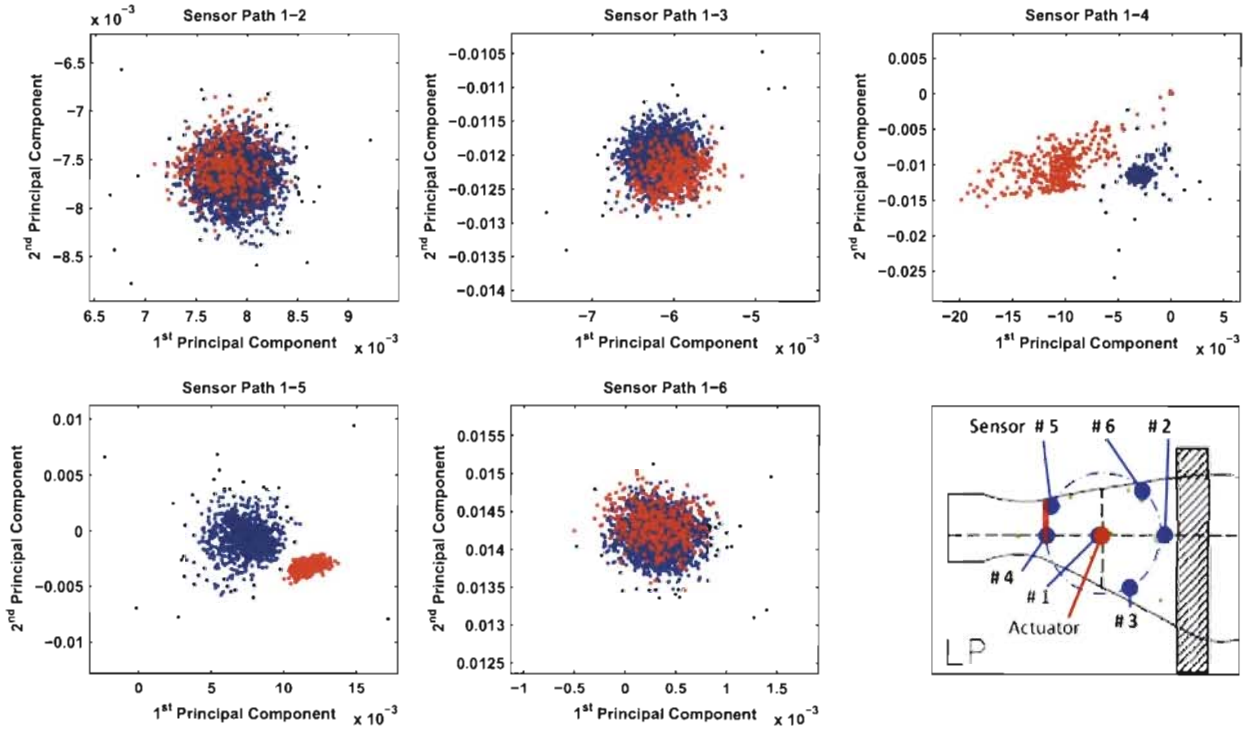

Figure 10. WASP ARX-PCA results for the low-pressure side array.

4.2 Frequency Domain Correlation Coefficient

Using the LASER system, diffuse wave-field frequency response functions were measured from 0.5 kHz to 40 kHz, with a sampling rate of 96 kHz. The cross-correlation (CC) between a newly measured FRF and a baseline FRF was computed, and the feature was taken as unity minus this CC value ($1-CC$). If the newly measured FRF is the same as the baseline, the value $1-CC$ will be zero, but if the underlying structure has changed (e.g. if damage occurs), the value will increase. The values of the $1-CC$ feature are plotted versus test number in Figure 11 for the LASER Inner array, and in Figure 12 for the LASER Outer array. There are noticeable increases in the (1-CC) feature for all sensor paths in the inner array after 10/20/12 (corresponding to test 280 in Figure 11 and Figure 12), but for the outer array, there appeared to be no significant change until the blade underwent catastrophic damage.

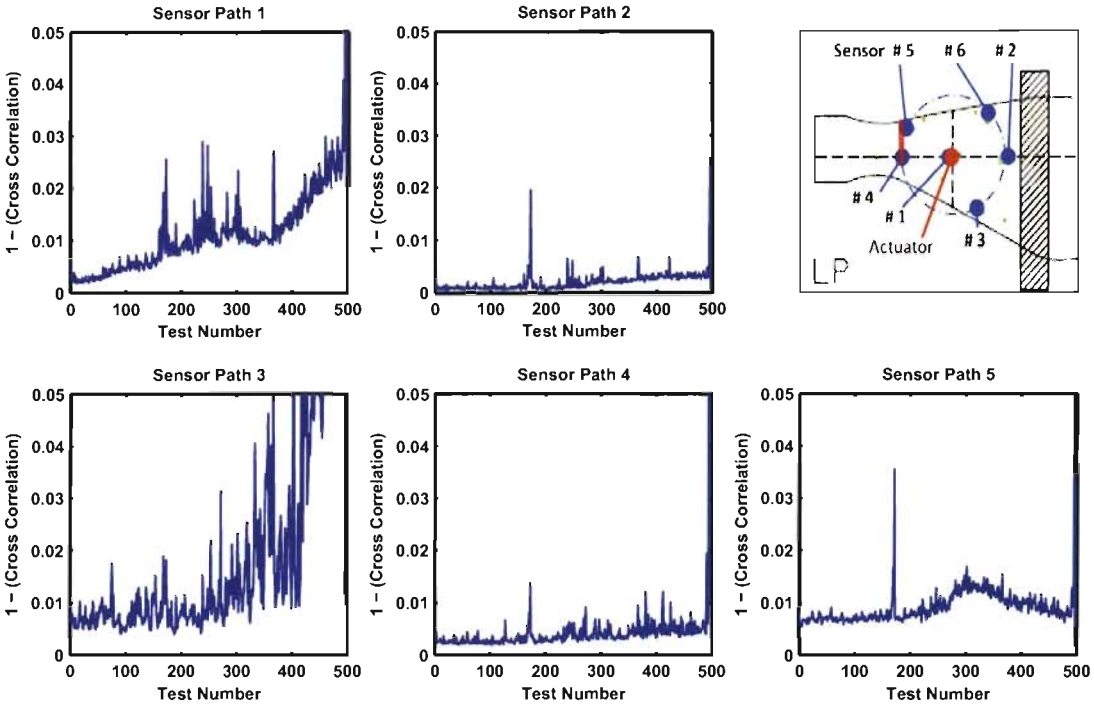

Figure 11. Cross correlation-based feature results for the LASER inner array.

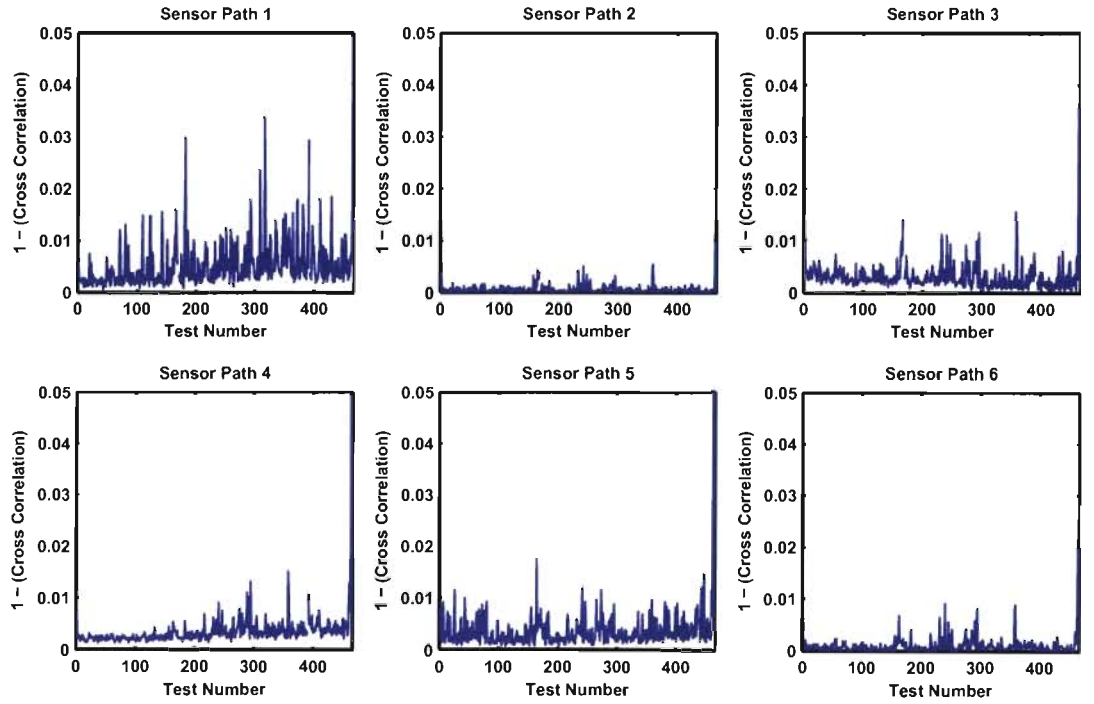

Figure 12. Cross correlation-based feature results for the LASER outer array.

5. SUMMARY

A sampling of data analysis methods have been presented and assessed for their ability to detect fatigue crack damage in a CX-100 wind turbine blade. Some of the methods and/or datasets appear insensitive to the crack's presence, while others may be overly sensitive, responding strongly to the crack's presence irrespective of the sensor path's proximity to the crack. The results of this study will be used to drive algorithm development and excitation and sensing methods for an upcoming flight test of a CX-100 blade.

The data from which the results presented in this paper were computed will be made available on the LANL Engineering Institute website: http://institute.lanl.gov/ei/software-and-data.

ACKNOWLEDGEMENTS

This research was funded by the Department of Energy through the Laboratory Directed Research and Development program at Los Alamos National Laboratory, as well as by the Leading Foreign Research Institute Recruitment Program through the National Research Foundation of Korea funded by the Ministry of Education, Science and Technology (2011-0030065). The authors would also like to acknowledge Scott Hughes and Mike Desmond from National Renewable Energy Laboratory, and Mark Rumsey and Jon White from Sandia National Laboratory for their support and guidance on this study.

REFERENCES

[1] S. G. Taylor, K. M. Farinholt, E. B. Flynn *et al.*, "A mobile-agent-based wireless sensing network for structural monitoring applications," Measurement Science and Technology(4), 045201 (2009).

[2] S. Taylor, K. Farinholt, G. Park *et al.*, "Multi-scale wireless sensor node for health monitoring of civil infrastructure and mechanical systems," Smart Structures and Systems, 6(5-6), 661-673 (2010).

[3] S. G. Taylor, J. Carroll, K. M. Farinholt *et al.*, [Embedded processing for SHM with integrated software control of a wireless impedance device] SPIE, San Diego, CA, USA(2011).

[4] D. Berry, "Design of 9-Meter Carbon-Fiberglass Prototype Blades: CX-100 and TX-100," SAND2007-0201, Sandia National Laboratories, Albuquerque, NM, (2007).

[5] K. M. Farinholt, S. G. Taylor, G. Park *et al.*, [Full-scale fatigue tests of CX-100 wind turbine blades. Part I – testing] SPIE, San Diego, CA(2012).

[6] P. Gyuhae, R. F. Charles, S. Francesco Lanza di *et al.*, "Performance assessment and validation of piezoelectric active-sensors in structural health monitoring," Smart Materials and Structures, 15(6), 1673 (2006).

[7] S. G. Taylor, K. M. Farinholt, G. Park *et al.*, [Wireless impedance device for electromechanical impedance sensing and low-frequency vibration data acquisition] SPIE, San Diego, CA, USA(2009).